J Mol Model (2013) 19:3187–3200
DOI 10.1007/s00894-013-1849-1

ORIGINAL PAPER

Thermodynamic computational approach to capture molecular recognition in the binding of different inhibitors to the DNA gyrase B subunit from *Escherichia coli*

Liane Saíz-Urra · Miguel Ángel Cabrera Pérez · Matheus Froeyen

Received: 20 July 2012 / Accepted: 4 April 2013 / Published online: 30 April 2013

Abstract DNA gyrase subunit B, that catalyzes the hydrolysis of ATP, is an attractive target for the development of antibacterial drugs. This work is intended to rationalize molecular recognition at DNA gyrase B enzyme – inhibitor binding interface through the evaluation of different scoring functions in finding the correct pose and scoring properly 50 *Escherichia coli* DNA Gyrase B inhibitors belonging to five different classes. Improving the binding free energy calculation accuracy is further attempted by using rescoring schemes after short molecular dynamic simulations of the obtained docked complexes. These data are then compared with the corresponding experimental enzyme activity data. The results are analyzed from a structural point of view emphasizing the strengths and limitations of the techniques applied in the study.

Keywords Escherichia coli DNA gyrase inhibitors · MM-GBSA · MM-PBSA · Molecular docking · Molecular dynamics simulations · Rescoring techniques

Introduction

The continuing drug resistance developed by bacteria justifies the need to investigate new antibacterial targets that could lead to the design of drugs with a novel mechanism of action and without resistance issues [1]. Still, finding an appropriate antibacterial lead using a target-based screening approach is not an easy and cheap task [2]. A more affordable strategy is to investigate validated antibacterial targets searching for new agents with different binding modes so that known mechanisms of resistance do not affect their inhibitory effect.

DNA gyrase is one example of a target that can be used for this kind of strategy [3]. It is an essential prokaryotic type II topoisomerase enzyme with no direct mammalian equivalent that introduces negative supercoiling in DNA at the expense of ATP hydrolysis. It participates in DNA replication, transcription, and recombination. DNA gyrase is a tetrameric enzyme, each monomer having two subunits, GyrA and GyrB. The A subunit of DNA gyrase is involved in DNA breakage and reunion while the B subunit catalyzes the hydrolysis of ATP [4]. Inhibitors of GyrB bind to the ATP binding pocket in the N-terminal domain of GyrB competing with ATP which causes the interruption of DNA synthesis and further cell death [4]. The novobiocin reached the clinical phase but was withdrawn from clinical use due to toxicity issues [5]. At the moment no commercial antibiotic targets the B subunit of gyrase. However, new chemotypes have been identified. An example is the last structures of the Staphylococcus aureus GyrB ATPase domain in complex with pyrrolamide inhibitors deposited in the Protein Data Bank (PDB) with the codes 3U2K, 3U2D and 3TTZ [6, 7] by Prof. A.E. Eakin and colleagues.

The mode of action of many drugs is related to the activation or inhibition they exert on biological targets. Design of new small compounds that bind the receptors with high inhibition strength can be guided by an *in silico* study of thermodynamic properties like the binding free energy $\Delta G°$. The application of this strategy to the design of new ATPase inhibitors is given by the work of Schechner

Electronic supplementary material The online version of this article (doi:10.1007/s00894-013-1849-1) contains supplementary material, which is available to authorized users.

L. Saíz-Urra · M. Froeyen (✉)
Laboratory for Medicinal Chemistry, Rega Institute for Medical Research, Katholieke Universiteit Leuven,
Minderbroedersstraat 10, 3000 Leuven, Belgium
e-mail: mathy.froeyen@rega.kuleuven.be

L. Saíz-Urra · M. Á. C. Pérez
Centro de Bioactivos Quimicos, Universidad Central de Las Villas,
Carretera a Camajuani km 5 1/2 Santa Clara,
Villa Clara 54830, Cuba

et al. [8] where a consensus map was built by calculating the binding free energy of different functional groups to indicate binding sites that are insensitive to the specific protein conformation. Yu and Rick have reported the use of thermodynamic integration computer simulations to calculate the free energy, enthalpy and entropy for the water molecules involved in hydrogen bonds with the inhibitors novobiocin and clorobiocin and polar atoms of certain residues in the ATP active site [9]. Brvar et al. [10] reported a novel class of 2-amino-4-(2,4-dihydroxyphenyl)thiazole based inhibitors with low micromolar antigyrase activity. They combined molecular docking calculations with three-dimensional structure-based pharmacophore information derived from the available description of the cyclothialidine GR122222X binding mode.

In order to contribute to the drug discovery process of new antibacterial agents, we attempt to evaluate in this work the capability of different scoring functions to score a set of *Escherichia coli* DNA GyrB inhibitors. The possible improvement of the binding free energy calculation is further explored by using rescoring schemes after short molecular dynamic simulations of the obtained docked complexes. The results are compared with the corresponding experimental enzyme activity data and discussed in detail from a structural standpoint identifying the strengths and limitations of these techniques when applied to the prediction of DNA GyrB inhibition.

Materials and computational details

Data set

A set of 50 compounds was used in the study (see Fig. 1). Specifically five indazole analogues [11], 16 4-amino-pyrazolopyrimidine analogues [12], 13 cyclothialidine derivatives [13, 14] and 16 novobiocin derivatives [15–18] were used to model the inhibition of the *E. coli* DNA GyrB subunit (see Table S1 in the Supplementary material for structural detail of every compound).

The experimental enzyme activity data have been reported elsewhere describing the in vitro supercoiling assay where the

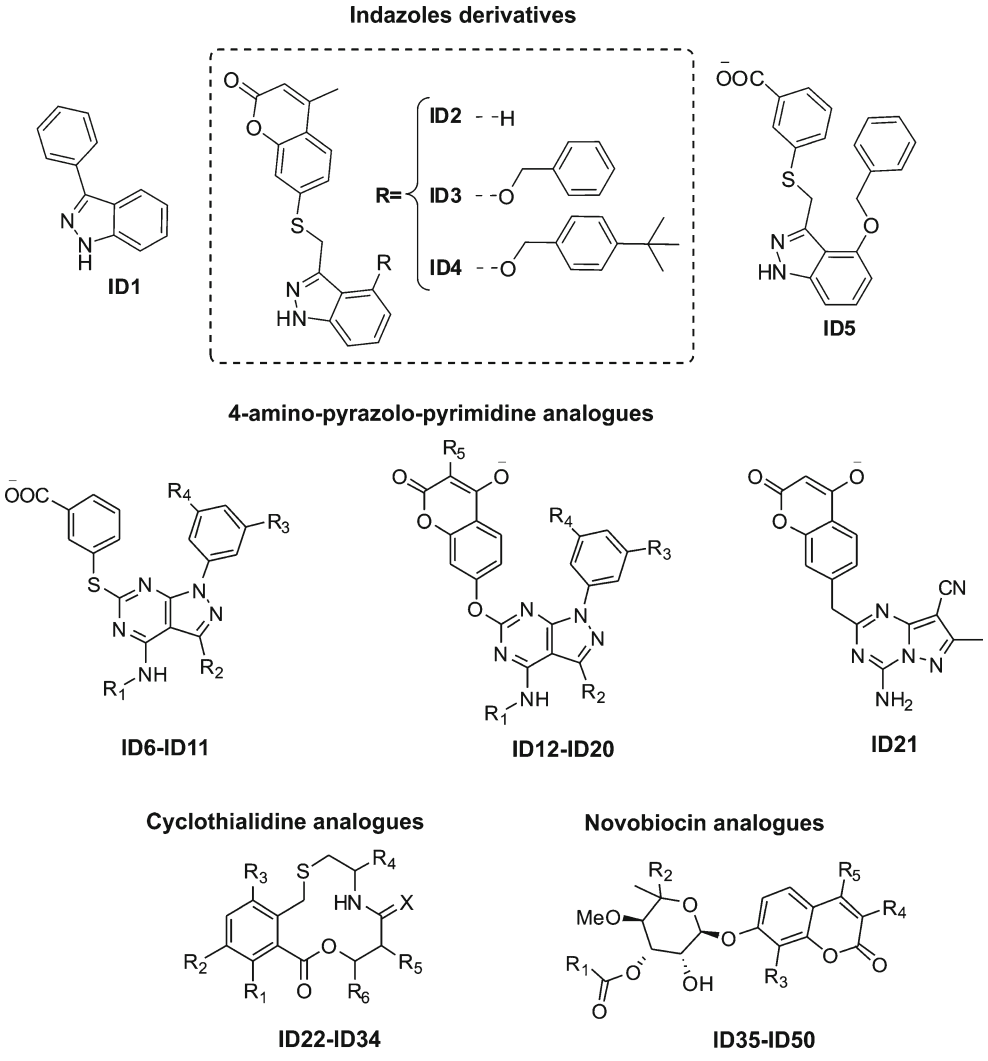

Fig. 1 General structure of the compounds used in the study

introduction of superhelical turns into a relaxed plasmid (plasmid and enzyme from *E. coli*) is determined by gel electrophoresis and expressed as the maximum noneffective concentration (MNEC in μg mL^{-1}) [11] [12] [13, 14] or the concentration of a drug that is required for 50 % inhibition in vitro (IC_{50} in μg mL^{-1} only in the case of the novobiocin derivatives) [15–18].

We also collected six crystallographic structures of DNA GyrB complexed with five different inhibitors. The inhibitors with their ID in the dataset, PDB code, organism and resolution of the x-ray structure are: I) novobiocin(ID50) (1AJ6 [19] PDB code, *E. coli*, 2.30 Å and 1KIJ [20] *Thermus thermophilus* 2.30 Å); II) clorobiocin(ID44) (1KZN [21] *E. coli*, 2.30 Å); III) GR122222X(ID34) [22] kindly provided by Prof. D. Wigley (*E. coli*, 2.10 Å); IV) one indazole [11] (3-((4-(benzyloxy)-1H-indazol-3-yl)methylthio)benzoic acid (ID5), 12b24.pdb *Staphylococcus aureus*, 2.36 Å) and V) one 4-amino-pyrazolopyrimidine [12] (3-(4-amino-1-(3,5-dichlorophenyl)-3-ethyl-1H-pyrazolo[3,4-d]pyrimidin-6-ylthio) benzoic acid (ID8), 13b24.pdb *Staphylococcus aureus* 2.3 Å) from Prof. D. Kostrewa.

Ligand preparation

The 50 molecules were sketched in the ChemDraw Ultra [23] software package and their SMILES notations were generated. The 3D structure of the compounds was built with programs from OpenEye Scientific Software Inc, makefraglib and OMEGA version 2.3.2 [24]. Atomic partial charges were assigned using the AM1BCC partial charge model from the Molcharge software included in QUACPAC version 1.3.1 (QUality Atomic Charges, Proton Assignment and Canonicalization) [25]. The structure of the GyrB subunit complexed with cyclothialidine GR122222X was used as the query file to specify the coordinates for the core substructure of the cyclothialidine-like input molecules. The protonation of the ligands was defined using the calculator plugins for pKa included in MarvinSketch 5.4.1.1[26].

Receptor preparation before the molecular docking experiment

Following the fact that the flexible loop 2 of the GyrB has been described to be in an open conformation in complexes involving phosphate free compounds [27], the use of this structure seems to be a rational approach to apply in virtual screening of possible GyrB inhibitors. For this purpose, the coordinates for the receptor structure were taken from the crystal structure of the *E. coli* GyrB—clorobiocin (CBN) complex, PDB code 1KZN [21]. The missing coordinates of the flexible loop 1 (residues His83 to Glu86) were taken from the PDB entries 1EI1 [28] (*E. coli* GyrB43-ADPNP structure). Since these residues are identified as His82A, Pro82B, Glu82C and Glu82D in the 1KZN file when reporting missing residues, a conversion of the numbering of residues between Gly83 and Ala96 into Gly87 and Ala100 was executed to match the numbering in the *E. coli* sequence described so far.

On the other hand, the missing coordinates of loop 2 (residues Gly101 to Val118 in *E. coli*) were taken from the PDB entry 1KIJ [20] (*T. thermophilus* GyrB43-NOV) based on the facts that both have an open conformation and that both species show about 77.8 % of sequence identity in that region (14 out of 18 residues are the same) [20]. The Dali server was used for superimposing the structures from 1EI1 and 1KIJ with the one from 1KZN for extracting coordinates of loop 1 and loop 2 respectively. The pertinent mutations were carried out in the case of loop 2 as described in a previous work [29].

A short MD simulation was performed including the clorobiocin (CBN) ligand to stabilize the loops while keeping the rest of the protein restrained as previously reported [30]. A crystal water molecule (HOH1 in 1KZN), that has been reported to be conserved in the complex of DNA gyrase B with ATP and other inhibitors, was kept in the receptor structure [11, 20–22, 31–34].

Docking experiments. Scoring and rescoring calculations

Autodock4.2 [35] was used to look for the best poses while docking the different ligands in the active site. Autodock4.2 atom types were assigned to the protein and ligand structures and Gasteiger charges were added to the receptor. The protein and ligand structures were saved only with polar hydrogens (the hydrogens which are bound to C were united into the carbons) in the PDBQT format by using AutoDockTools (ADT) version 1.5.4 [36]. All possible torsions were activated in the ligands and amides were allowed to rotate.

Different grid boxes were generated with ADT. The first box was set based on the binding site defined by all the protein residues within 6 Å from the atoms of the two biggest inhibitors (clorobiocin and GR122222X) of the data base whose x-ray coordinates were at our disposal. This grid box had the center in position (26.002 Å, 37.59 Å, 36.35 Å) with 38, 56 and 44 points in the x, y and z dimensions respectively with spacing step of 0.375 Å. Six more boxes were generated by increasing the size (i.e., increasing number of points in the x, y and z dimensions but keeping the spacing step of 0.375 Å) to explore the possible influence of the defined binding pocket on the docking simulations. The description of every box used in the analysis is given in Table 1.

The Lamarckian genetic algorithm was run 50 times per molecule under the following conditions: number of individuals in population equal to 150, maximum number of energy evaluations 2,500,000 and maximum number of generations 27,000. The protein structure was considered as rigid during the docking. The other Lamarckian genetic algorithm parameters related to the local search were set to the default values proposed in the Autodock program.

The pose prediction accuracy of the five inhibitors whose crystallographic structures were available was assessed by the root mean square deviation (RMSD) of the docked structure from the crystal structure. A threshold value of 2.0 Å was considered for defining the docked pose successfully. The binding pose of the rest of the compounds (nine-tenths of the data set) was evaluated following the ideas behind the interactions-based accuracy classification (IBAC) scheme described by Kroemer et al. [37]. According to this, the quality of the predicted pose is ascertained by visually comparing to the crystallographic reference structure regarding the hydrogen-bonded and other key ligand-protein interactions by parts, first the scaffold and then the remaining fragments. The pose was deemed correct in case of conserving all the key interactions, nearly correct when some relevant interactions (up to a quarter) were not reproduced and incorrect if more interactions are missing.

Only random starting conformations of the ligands were used as input to perform the docking experiments. The visual analysis of the poses of the docked ligands and their interactions with the protein, especially the hydrogen bonding network as well as all the molecular graphics images were performed using the UCSF Chimera package [38]. Figures in this manuscript describing binding modes of the ligands are shown in 3D using wall eye stereo camera for better understanding.

The scoring functions Shapegauss [39], PLP[40], Chemgauss3, Chemscore [41], OEChemscore and Screenscore [42], available in the Fast Rigid Exhaustive Docking (FRED) program, were used to score the best docked poses from Autodock4.2 in order to explore their performance in correlating the activity values and the predicted binding energies. In addition, the Zapbind function [43] was used to rescore the molecules. This is a function that combines a surface area contact term and an electrostatic interaction calculated using the Poisson-Boltzmann (PB) solvent approximation.

For this aim the receptor was prepared by using the FRED receptor program version 2.2.5 [44]. The conditions will be explained in terms (put in quotation marks "") of this software's graphical interface.

The ligands clorobiocin and GR122222X were kept in the receptor to define the active site. The docking site detection was done using the "molecular method" that is based on multiple molecular probes which are small molecules representing the shapes of druglike molecules. The docking event is more favorable in those regions where more probes dock. The top docking scores of the probes are used to generate a shape potential field which is the negative image of the active site and it is used as a first quick filter to select the best docking poses of the ligand molecules [44–46]. The quality of the shape potential was defined as "medium" following the reasons described in our previous work [30]. The resulting box volume was 10,080 $Å^3$, with contours of 61 $Å^3$ inner and 1699 $Å^3$ outer. The final receptor was saved considering the hydrogen bond constraint with Asp73 residue and the conserved crystal water molecule (HOH1 in 1KZN). The docking solutions obtained by Autodock4.2 (i.e., the best pose found for the compounds), were first refined using the Merck molecular mechanics force field [47] and then scored by the different scoring and rescoring functions included in FRED and previously mentioned here. This refinement allows a full coordinate optimization of the ligand atoms while the protein is held rigid providing a fairer basis for the comparison of the performance between the scoring/rescoring functions under analysis [48].

Molecular dynamics simulation and MM-PBSA/MM-GBSA as rescoring functions

Molecular mechanics—Poisson-Boltzmann surface area (MM-PBSA) [49] and generalized Born (MM-GBSA) [50, 51] are endpoint methods that combine molecular mechanics and continuum solvent calculations to analyze binding free energies. Usually, conformational ensembles from a single molecular dynamics simulation of a complexed system in explicit water are used to extract the conformational snapshots for complex, ligand and receptor that will be combined with a continuum solvent model to calculate their free energy contributions [52].

The binding free energy is then calculated as the difference between the energy of the complex and the two unbound binding parts. The energy of every component is considered as the sum of the vacuum and the solvation energy. The vacuum energy term comprises the enthalpy, calculated by the molecular mechanics force field, and also the gas phase entropy which has translational, rotational and vibrational contributions being the last one determined by normal mode analysis. The solvation free energy contributions are calculated using a continuum solvent model where the electrostatic component is estimated by the Poisson-Boltzmann formulation or the alternative generalized Born

Table 1 Information about the different grid box generated by using ADT

Box number	Center position	Number of points in the x, y and z dimensions
1	26.00 Å, 37.59 Å, 36.35 Å	38×56×44
2	26.00 Å, 36.80 Å, 37.00 Å	40×60×48
3	26.00 Å, 36.80 Å, 37.80 Å	40×60×52
4	26.00 Å, 36.80 Å, 37.50 Å	42×60×54
5	25.40 Å, 36.80 Å, 37.50 Å	46×60×54
6	25.40 Å, 37.50 Å, 37.50 Å	46×64×54
7	26.00 Å, 37.59 Å, 36.35 Å	60×64×60

model and the non-polar contribution to the solvation is linearly dependent on the **s**olvent **a**ccessible **s**urface **a**rea (**SASA**) [53].

In this work, MD simulations of the resulting docked structures were performed by using the AMBER package (version 10) [54] considering the protein or the ligand free of constraints as described in more detail in our previous work [29]. The Antechamber program [55] was used for the preparation of the ligands. The general AMBER force field (GAFF) was chosen for the ligands [56] and the ff03 force field for the protein [57, 58]. The explicit water model consisted in a truncated octahedral box of water molecules (TIP3PBOX) [59] keeping at the same time the conserved water molecule also included in the docking experiment. Na + ions were added for electrostatic neutrality. The assignment of the protonation state of the histidine residues in the active site was done based on the pKa calculations for the wild type protein reported by Schechner et al. [8], which also has been used by Yu et al. [9]. The protonation of the histidine residues in the active site was as follows (*E. coli* PDB numbering): 37 HID, 38 HIP, 55 HIE, 64 HIE, 83 HIE, 99 HIP, 116 HIP, HID136, 141 HIE, 147 HIP, 215 HIE, and 217 HIP, (HID is the Nδ tautomer, HIE is the Nε tautomer, and HIP is doubly protonated) [8, 9, 29]. We followed the typical scheme of the simulation covering the minimization and heating as well as the equilibration process of the system first at constant volume and switching then to constant pressure as described in our previous work [29]. The production simulations covered a period of 2 ns in total with a time step of 2 fs. Long-range electrostatics interactions were estimated by the particle mesh Ewald (PME) method [60] with a non-bonded cut off distance of 10 Å. The covalent bonds with hydrogen atoms were constrained applying the SHAKE method [61]. Periodic boundary conditions were applied to all dimensions. After equilibration, coordinates were saved every 200 steps (0.4 ps) for a total of 5000 snapshots collected. Enthalpy calculations were performed using 2500 snapshots from 2 ns of the molecular dynamics simulations with 0.8 ps time intervals. Due to the computational expense of the nmode calculations, entropy was calculated using 20 snapshots from molecular dynamics simulations with 100 ps time intervals.

Results and discussion

Molecular docking results. Binding mode analysis

After running molecular docking simulations under the different grid box conditions, the successful reproduction of the binding mode of the five reference compounds whose crystallographic structures were available (ID5, ID8, ID34, ID44 and ID50), was assessed by estimating the RMSD. The results of this experiment are shown in Table 2.

As can be seen, only the use of box 1, with the smallest size, led to RMSD values lower than 2 Å for every reference compound. Using other boxes we found deviations mainly in the poses predicted for compounds like novobiocin (ID50), cyclothilidine compound GR122222X (ID34) and the pyrazolopyrimidine ID8. For example, the deviation of the docked poses of novobiocin was found in the coumarin and butenylbenzamide substructures. In the cyclothilidine compound GR122222X (ID34), the positions of the resorcinol and 12-membered lactone ring moieties were close to the one found in its crystallographic structure but the R5 substituent (−NH-3Hyp-Ala, see Table S1 for structural details) showed deviations. The most critical case was the binding prediction of the pyrazolopyrimidine ID8. By increasing the size of the original box it was found that the pyrazolopyrimidine was predicted to be posed closer to the surface of the cavity thereby loosing the hydrogen bond with Asp73.

Despite that the definition of box 1 can seem narrow to properly accommodate all selected ligands, all the residues forming the cavity of the protein, including part of loop 2, are contained in this box. By increasing the size of the box, we include other residues from loop 2 (in open conformation) and in general, more surface of the protein that are supposed to be in contact with the solvent (which is not taken into consideration explicitly in the docking experiments) and are not part of the cavity. This increment is not efficient and can lead to the distortion of the pose of substituents of compounds like novobiocin and GR122222X (see Fig. S1 in the Supplementary material for graphical representation of different boxes).

Based on the accurate reproduction of the binding mode of the reference compounds by using grid box 1 we decided to apply the same conditions in the docking simulation of the rest of the compounds in the data set.

Following the IBAC scheme described by Kroemer et al. [37] the interactions established by the rest of the compounds in the active site were compared to the ones established by the crystallographic references analyzing first the scaffold and then the remaining fragments of the molecules. Those compounds whose scaffold differed from the ones of the respective reference in chirality were not assessed by this scheme. The most important interaction included in the derivation of IBAC criterion to classify a pose as correct was the hydrogen bond between the conserved water molecule (HOH1), Asp73 and the ligands. Such interaction pattern was observed in most of the compounds. In general, the pose found by molecular docking for these compounds was classified in the majority of the cases as correct since all the key interactions with the protein were displayed. The other interactions considered for the classification of the pose are explained next in details for every subset of congeneric compounds.

Table 2 Parameters resulting from the Autodock4.2 molecular docking simulations of the five reference structures in the data using seven different grid boxes

ID	Parameters[a]	Box number						
		1	2	3	4	5	6	7
ID5	RMSD	**1.05**	2.38	**1**	**1.44**	**0.9**	**1.81**	**1.24**
	Rank	1	1	1	1	1	1	1
	Energy	**−9.15**	−8.90	−8.84	−8.67	−8.94	−9.02	−8.89
ID8	RMSD	**0.84**	5	4.69	4.65	–	4.82	3.66
	Rank	1	22	24	24	–	23	16
	Energy	**−9.78**	−6.46	−6.30	−6.34	–	−6.20	−6.61
ID34	RMSD	**1.66**	2.54	2.1	2.25	2.64	2.42	3.29
	Rank	1	1	1	1	1	1	1
	Energy	−10.64	−11.25	−11.38	−12.38	−12.17	−11.19	−10.33
ID50	RMSD	**1.5**	4.32	2.75	2.63	6.74	4.32	2.68
	Rank	1	6	7	5	2	6	5
	Energy	**−7.42**	−6.02	−6.02	−6.23	−6.46	−6.67	−6.67
ID44	RMSD	**1.7**	**1.84**	**1.84**	4.11	4.26	4.63	**1.56**
	Rank	2	2	2	1	2	25	3
	Energy	**−8.75**	−7.25	−7.26	−8.33	−7.68	−5.38	−8.67

[a]Rank and energy are related to the Autodock4.2 search algorithm output models

In the case of the pyrazolopyrimidine analogues (ID6-ID21), π-stacking to the salt bridge Arg76-Glu50 [62] either from 4-hydroxy-coumarin or a 3-mercapto benzoic acid substituent was predicted. The phenyl group linked directly to the pyrazole moiety was involved in lipophilic interactions with Ile94. The acid group of 3-mercapto benzoic acid derivatives established ionic interactions with Arg136 while analogues with 4-hydroxy-coumarin substituents interacted with this residue by hydrogen bonding. Bigger substituents (in comparison with the ones in the reference structure) as acetamide and butylurea ($-NHCONH(CH_2)_3CH_3$) were located in a similar pocket as the isopentenyl group of the novobiocin (NOV) inhibitor. Substituents on the amino group of the pyrazolopyrimidine analogues like cyclopropyl (compounds ID9 and 15) and ethyl (compound ID10) interacted in the region of the hydrophobic pocket with residues Val43, Ala47, Val71, Gln72 and Val167, similar to the methylpyrrole ring of ligand clorobiocin (CBN) (see Fig.S2 in the Supplementary material).

The binding mode of indazole analogues (ID1-ID5) resulted similar to the one predicted for the pyrazolopyrimidines given the common substituents these subsets share; coumarin fragment and 3-mercapto benzoic acid. Only in the case of 3-phenyl-1H-indazole (compound ID1) the orientation differed from the rest of the compounds in this subset. At first sight compound ID1 could be classified as incorrect but since its structure differs to a large extent from the reference ID5 because of the phenyl group attached directly to the indazole, we considered that we did not have enough information for classification. Its best pose is predicted to be anchored in a deep hydrophobic pocket enhancing hydrophobic interactions between the indazole and the residues Gln72, Val71, Val167 and Val43. The phenyl substituent interacts with Met95 and Val120. Nevertheless, the hydrogen bond between the NH group of the indazole and Asp73 is observed (Fig. 2).

When analyzing cyclothialidine derivatives, the positions of the resorcinol and 12-membered lactone ring moieties (ID22-ID34) were found to be similar to the one in the GR122222X reference and comparable to previous docking reports [63, 64]. However, both predictions present shifted lactone ring hydrogen bonding the Asn46 side chain NH_2 which is not observed in the reference GR122222X-GyrB x-ray structure since the Asn46 amide side chain has a 180° flipped conformation regarding the docking receptor structure (see Fig. S3 and S4 in the Supplementary material). We considered then the pose predicted for these compounds as nearly correct.

The binding mode predicted for the novobiocin analogues (ID35-ID50) was very similar to the one of the reference crystallographic structures of novobiocin and clorobiocin which has been described in detail before [19, 22, 27, 65]. Lamarckian GA reproduced the bent conformation of the butenylbenzamide substituent starting from a random generated input structure.

The best pose ranking achieved by using Autodock4.2 ranged between 1 and 3 for all the compounds of the data set (see Table S2 of Supplementary material).

Activity vs. Scoring. Molecular dynamics simulations. Rescoring functions. Good news?

Table 3 shows the correlation coefficients between the scaled values of DNA supercoiling inhibiting activity (log(Activity)) and the scoring function energy values for every congeneric set of compounds. All experimental enzyme activity data was converted from μg mL^{-1} into μM

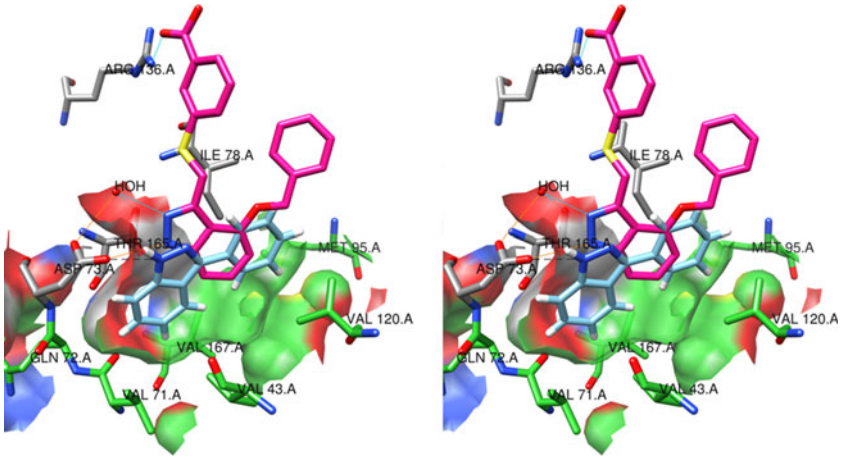

Fig. 2 Binding mode prediction for indazole ID1. Carbon atoms of the reference ligand (ID5) are in magenta color and the ones of compound ID1 are in light blue. The interacting residues are in green as well as their surface

units for a better correlation with the kcal mol^{-1} units counting for the energy (for individual scoring function values see Table S2 of Supplementary material).

The performance of the scoring functions varied from one subset to another. The strongest correlation was found for the indazole analogues by using the scoring function from Autodock4.2 (R=0.896) as well as a correct ranking-order. This was followed by Chemgauss3 scoring function in the case of cyclothialidine like compounds (R=0.755). Pyrazolopyrimidine and novobiocin analogues were considered lack of any correlation. As can be seen, the molecular docking algorithm used in the study had a better performance predicting the correct binding poses, which in many cases was identified as the best-docked pose with the lowest energy, than predicting binding affinities.

Improved correlations were found when using rescoring functions for indazole and pyrazolopyrimidine analogues. However, for cyclothialidine compounds, the rescoring correlation was lower (MM-PBSA R=0.628) when compared to the scoring functions Chemgauss3 (R=0.755), Autodock4.2 (R=0.645) and Screenscore (R=0.650).

The MM-PBSA method performed better than the rest of the rescoring functions except for the pyrazolopyrimidine analogues where the correlation when using Zapbind was slightly higher (R=0.417; MPBSA R=0.399) (for individual rescoring function values see Table S3 of Supplementary material). To find the source of the problems in the correlations, we will discuss every subset separately.

Indazole analogues subset (ID1-ID5)

Autodock4.2 was the only one able to predict compound ID4 as the most active one thus perfectly ranking the indazole analogues (ID1-ID5) subset. Moreover, the favorable effect of the refinement applied to the structure before using the Zapbind function and the MM-PB(GB)SA rescoring led to enhanced interactions thereby improving the correlation and the ranking of the compounds of this subset.

In general all the scoring and rescoring functions recognized the more favorable effect of the bicyclic coumarin over the monocyclic benzoic acid moiety (ligands ID3 and ID5 respectively). This is an example of expected successful

Table 3 Values of calculated correlation between scoring and rescoring functions with the activity for every subset of compounds in the study

	Indazoles derivatives	Pyrazolopyrimidine analogues	Cyclothialidine derivatives	Novobiocin derivatives
Compounds	ID1-ID5	ID6-ID21	ID22-ID34	ID35-ID50
Autodock4.2	0.896	−0.167	0.645	0.082
Shapegauss	0.566	0.082	0.427	0.155
PLP	0.568	0.133	0.584	0.168
Chemgauss3	−0.103	−0.098	0.755	0.078
Chemscore	0.76	0.123	0.622	0.107
OEChemscore	0.579	0.006	0.538	0.097
Screenscore	0.384	0.295	0.650	0.220
Zapbind	0.84	0.417	0.416	0.041
MM-PBSA ($\Delta G_{(PB)\text{-subt}}$)	0.972	0.399	0.628	0.142
MM-GBSA ($\Delta G_{(GB)\text{-subt}}$)	0.952	0.279	0.604	0.132

application of the rescoring methods in scoring/ranking since it is a very small subset where the compounds display significant structural differences leading to dramatic changes in the activity that are well captured by the functions.

Pyrazolo-pyrimidine analogues subset (ID6-ID21)

Both, scoring and rescoring functions overestimated the affinity of pyrazolopyrimidine analogues with alkyl substituents at the 4-amino group (cyclopropyl in ID9 and ID15, ethyl in ID10) which are experimentally around 30 and 14-fold less active than the reference analogue of this subset (ID8). Drawing an analogy with the methylpyrrole of clorobiocin inhibitor [29], these alkyl groups displace two water molecules (1021.water and 1046.water in the GyrB-ID8 x-ray structure, see Fig. S5 in Supplementary material) from the hydrophobic pocket. From experimental thermodynamic data reported for GyrB bound to coumarins clorobiocin and novobiocin [19, 21, 31, 66] it has been described how the more favorable enthalpy driven by keeping these water molecules upon binding of novobiocin to GyrB is affected by an entropic cost leading to a better binding free energy and activity for clorobiocin. Interestingly, the enzymatic activity data of pyrazolopyrimidine analogues under analysis show that alkylamino compounds are less active. These data suggest that freezing the alkyl substituents might cause entropic penalty comparable to keeping water in the pocket. To explore this, a new MD simulation was run with the docked conformation of 4-amino- pyrazolopyrimidine ID8 including the two crystal water molecules interacting with the amino group. The further calculation of its free binding energy was done by means of MM-PB(GB)SA methods (for enthalpy) and the normal mode method (for entropy). In addition, the entropy for 4-alkylamino-pyrazolopyrimidine analogues ID9, ID10 and ID15 was also estimated. Table 4 shows the results.

Although the predicted enthalpy energy for the GyrB-ID8 interaction was enhanced by including the ordered water molecules at the protein hydrophobic pocket-ligand interface ($\Delta\mathbf{G_{(PB)\text{-}subt}}$=−41.30 kcal mol^{-1} and $\Delta\mathbf{G_{(GB)\text{-}subt}}$=−43.09 kcal mol^{-1} without water; $\Delta\mathbf{G_{(PB)\text{-}subt}}$=−44.15 kcal mol^{-1} and $\Delta\mathbf{G_{(GB)\text{-}subt}}$=−52.83 kcal mol^{-1} with water) it did not surpass the enthalpy predicted for binding of 4-alkylamino derivatives.

Entropy evaluation helped to explain the activity ranking of the 4-alkylamino analogues. Among these alkylamino compounds, the higher binding free energy of ID9 (with ethyl) was given by a combination of a higher enthalpy, explained by the smaller size of the substituent decreasing hydrophobic contact in the pocket, and an entropic cost (similar to keeping water molecules in the GyrB-ID8 simulation) due to the freezing of a more flexible ethyl regarding the cyclopropyl group (in ID15 and ID9) upon complexation.

The effect of the protonation state of the 4-hydroxyl-coumarin pyrazolopyrimidines analogues on the MD simulations will be discussed together with the novobiocin analogues.

Cyclothialidine analogues subset (ID22-ID34)

The typical bias produced by the assignment of the more favorable score to larger compounds, due to the larger pair-wise interactions was found in most of the scoring functions (e.g., cyclothialidine Ro 09–1437 with ID33 in data, Table S2). One of the main issues in this subset is the scoring of different stereoisomers. The majority of the scoring functions identified as the most active steroisomer cyclothilidine analogues those ones with the C4(R) and C7(S) configuration in agreement with the enzyme activity data [67] (See Table S2). Compounds like ID25(C4(R)/C7(R)), ID26(C4(S)/C7(S)) were correctly ranked by the scoring functions while MM-PB(GB)SA method did not distinguish a significant difference in their energies (See Table S3). All the scoring and rescoring functions failed predicting the inactivity of compound ID27 with the C4(S)/C7(R) configuration. An additional problem was that no scoring or rescoring functions identified molecule ID32 as the most active compound in the subset.

Analyzing first the binding mode of compounds ID24 till ID27 it was seen that the methoxyformyl substituent (COOMe) was predicted to interact either with Arg136,

Table 4 Binding free energy values for 4-alkylamino (hydrophobic pocket water free) and 4-amino (including water) -pyrazolopyrimidines-GyrB complexes

ID	$\Delta G_{(PB)\text{-}subt}$	$\Delta G_{(GB)\text{-}subt}$	TS_{TOT}	$\Delta G_{(PB)\text{-}total}$	$\Delta G_{(GB)\text{-}total}$	−log(MNEC)
ID8	−44.15	−52.83	−22.26	−21.89	−30.57	−0.27
ID15	−45.39	−56.02	−17.64	−27.75	−38.38	0.88
ID9	−45.61	−53.86	−19.65	−25.96	−34.21	1.20
ID10	−41.90	−51.04	−22.06	−19.84	−28.98	1.21

TS_{TOT} is the total entropy parameter comprising the translational, rotational, and vibrational entropy of the solute (TS=temperature multiplying the entropy). $\Delta G_{(PB)\text{-}total}$ and $\Delta G_{(GB)\text{-}total}$ are the final binding free energy values that include the effect of the entropy. Values of energy are reported in kcal mol^{-1} units.

Arg76 and Pro79 when linked to C4(R) configuration (ID24 and ID25) or with Pro79 and Ile94 in the case of C4(S) (ligands ID26 and ID27). Furthermore, COOMe is affected by the C7 configuration. Though in all stereoisomers the carbamate group of the t-butoxyformamide substituent at C7 was predicted to interact with Phe104, the t-butyl fragment interacted whether with Asp49 for C7(S) configuration (ID24 and ID26) or close to residues of loop 2 like Asp105, Val118, Lys110 and Tyr109 for C7(R) (in ID25 and ID27). Compound ID25 is not close enough to Arg136 to establish hydrogen bonding with its COOMe substituent at C4(R). So far, these differences in the stereoisomer binding modes are reflected in the correct ranking predicted by the scoring functions for compounds ID24, ID25 and ID26. Conversely, during the MD simulations the t-butoxyformamide substituent at C7(S) (ID24 and ID26) gets a conformation similar to the one found in the docked conformation of compounds with C7(R) (ID25 and ID27) and rotations of the bond connecting the carbonyl group from the methoxyformyl substituent to C4 are observed. This might justify the similar energies predicted by the MM-PB(GB)SA for ligands ID24, ID25 and ID26. However, it seems that our models shift the lactone macrocycle of ID27 from the reference binding mode avoiding expected clashes but still displaying hydrophobic interactions that lead to overestimated energy score values.

On the other hand, compound ID32 is structurally similar to compounds ID30 and ID31. They have a 3-methyl-1,2,4-oxadiazol-5-yl attached to C4 and no substituent at C7. The main difference lies in that ID31 and ID32 are 6-thioxo lactones while ID30 is a 6-oxo lactone. ID32 also has a hydroxymethyl group at C8(S) of the lactone ring which is predicted to interact with residues Asn46 and Val118.

The scoring functions Autodock4.2 and Chemscore as well as the rescoring functions Zapbind and MM-PB(GB)SA could not rank these compounds predicting negative correlations between the two parameters, energy and activity, instead (Table 5, correlation Exp1 row).

Analysis of MD simulations of the GyrB-ID32 complex based on RMSD calculations showed that the most flexible regions comprised residues from loop 2 and Arg136 and Asn46 with its surrounding residues Lys110, Glu42 Val118 and Val120 (Fig. S6 in Supplementary material) where the Asn46 side chain is very exposed to the solvent. Therefore, the Asn46 side chain conformation was analyzed in the enzyme structure used in the docking experiments (from pdb entry 1KZN) and the crystallographic structure of the DNA gyrase bound to the inhibitor GR122222X.

In the 1KZN structure, the NH_2 from Asn46 side chain points to the protein-ligand interface establishing van der Waals interactions with the clorobiocin noviose sugar and a hydrogen bond with Water1162 while the main chain makes hydrogen bonds with residues Glu42, Val43 and Asp49. The Asn46 side chain NH_2 has the opposite orientation in the GyrB-GR122222X x-ray structure and is stabilized by a hydrogen bond with Glu42. The side chain carbonyl (CO-Ans46) displays van der Waals interactions with GR122222X. The Asn46 backbone interacts by hydrogen bonding with Glu50 and Water92 (see Fig. S7 in Supplementary material).

The MolProbity web service [68] was used then, to analyze the Asn46 side chain in the crystallographic structure of the DNA gyrase bound to the inhibitor GR122222X. The program REDUCE [68] that considers all-atom steric overlaps was used to pick out the residues that might be flipped to improve the quality of the structure. After analyzing the GyrB-GR122222X x-ray structure, there was no evidence that a flip for the Asn46 side chain was needed (Rotamer data 45.6 % (*m-80*) chi angles: 281.9, 276.3).

To study the effect of this flip on the scoring and rescoring we performed additional experiments. After manually rotating the Asn46 side chain in the docking receptor to obtain the same rotamer as in the x-ray GyrB-GR122222X complex, new molecular docking, MD simulations with further energy calculations were performed for ID30, ID31 and ID32 (see Table 5, Exp2 for results).

Table 5 Energy predictions for compounds ID30, ID31 and ID32 under the two different conditions of experiments

	log(MNEC)	Autodock4.2	Chemgauss3	Chemscore	Zapbind	$\Delta G_{(PB)\text{-subt}}$	$\Delta G_{(GB)\text{-subt}}$
ID32(Exp1)	−1.66	−7.97	−86.85	−21.81	−12.29	−31.68(5.69)	−41.36(3.53)
ID31(Exp1)	−1.33	−8.43	−83.81	−22.32	−12.03	−42.27(3.85)	−47.44(2.89)
ID30(Exp1)	−0.91	−8.12	−79.96	−22.61	−12.18	−44.31(3.50)	−47.94(3.05)
Correlation Exp1[a]	–	−0.25	1.00	−0.97	0.36	−0.90	−0.87
ID32(Exp2)	−1.66	−8.53	−88.76	−19.05	−18.91	−27.85(5.83)	−41.36(3.60)
ID31(Exp2)	−1.33	−8.34	−87.07	−21.03	−13.03	−39.35(4.24)	−46.51(3.10)
ID30(Exp2)	−0.91	−8.20	−85.05	−20.04	−13.01	−32.81(4.46)	−42.08(2.87)
Correlation Exp2[a]	–	0.99	1.00	−0.44	0.83	−0.37	−0.06

Exp1 and Exp2 denotes the conditions of the two experiments. Exp1 = NH_2 of Asn46 side chain pointing to the cavity; Exp2 = carbonyl of the Asn46 side chain pointing to the cavity. [a] Pearson r correlation coefficient between activity (log(MNEC) and scoring energy values from the different functions calculated for the sample containing only compounds ID30 to ID32

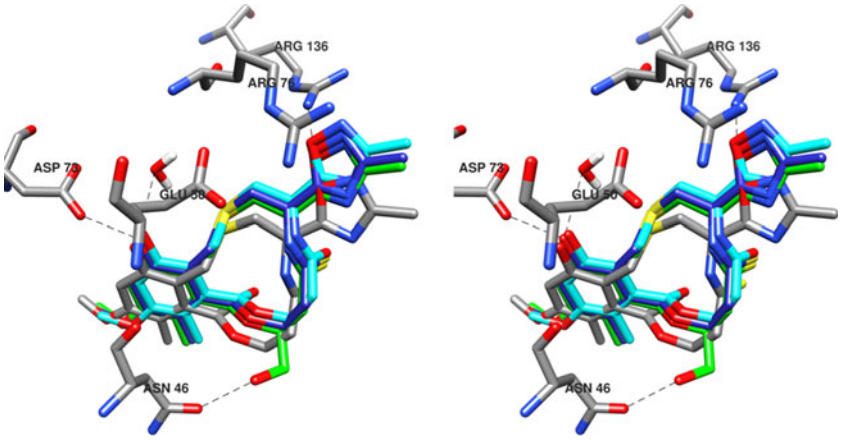

Fig. 3 Binding mode prediction for compounds ID30(*cyan carbons*),ID31 (*dark blue carbons*) and ID32 (*green carbons*) under the conditions of experiment 2. The binding mode predicted for compound ID31 (*element colored*) under conditions of experiment 1 has been display for comparison

After flipping the Asn46 side chain the new binding mode predicted for these compounds showed more resemblance to the reference regarding to the position of the macrocycle. The hydrogen bonding pattern between the 3-methyl-1,2,4-oxadiazol-5-yl substituent at C4 and Arg136 was found in all the complexes while ID32 was the only ligand able to make a hydrogen bond with the Asn46 side chain given its hydroxymethyl substituent making the difference in binding energy with the rest of the subset (see Fig. 3). In general, improvements in correlations were observed for the scoring and rescoring functions. It seems that the solvation parameter has a significant influence in the successful prediction of the binding energy of these compounds justifying the improvement in the predictions of scoring functions like Autodock4.2 [35] and Zapbind function [43], that include solvation parameter, with respect to Chemscore [41]. It is important to note the advantages of the Zapbind method in this subset over the MM-PB(GB)SA method which makes use of expensive MD simulations. Zapbind method is able to rank correctly these compounds when starting from a correct binding pose while the MM-PB(GB)SA results are negatively influenced by the fluctuations of some residues in the binding interface during the MD simulations.

Furthermore, Autodock4.2 was used to dock molecules clorobiocin, GR122222X and ID32 into the enzyme using the same protocol as before but considering the Asn46 side chain flexible. In all cases the docked solutions showed a flip in the Asn46 side chain leading to the rotamer observed in the Gyr-GR122222X x-ray structure in agreement with the MolProbity results.

Novobiocin derivatives subset (ID35-ID50)

The protonation state of the ligands had an important influence on the complex stability along the MD simulations and the relative binding free energy calculated by MM-PB(GB)SA methods in this subset. Based on the pKa values calculated by MarvinSketch 5.4.1.1, primary and secondary 4-amine-coumarin analogues were protonated (ID35 to ID37) while 4-hydroxy-coumarin were deprotonated (ID45 to ID49). However, the assignment of the protonation state was not trivial for 4-hydroxy-coumarin derivatives novobiocin and

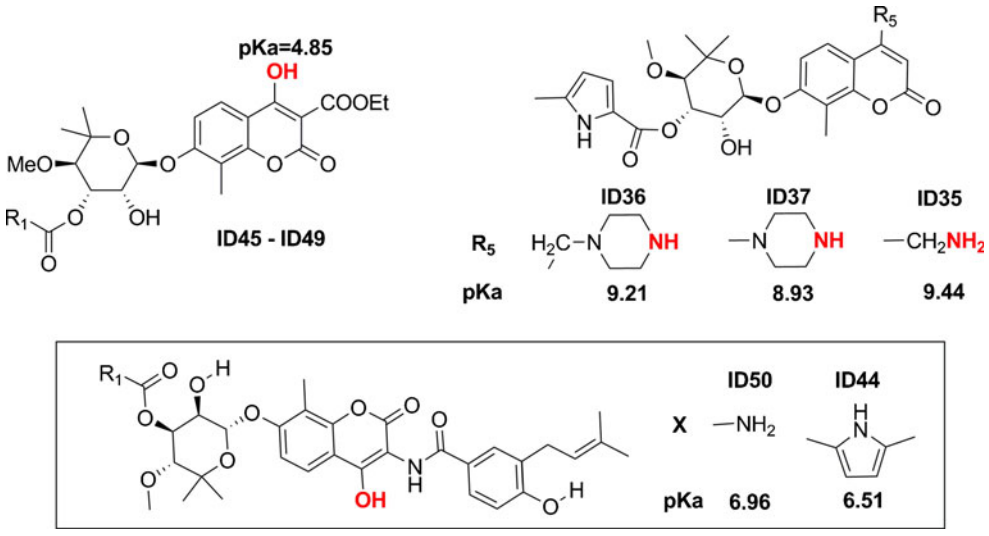

Fig. 4 pKa values calculated by MarvinSketch 5.4.1.1 to estimate the protonation state of the compounds in the subset

Table 6 Binding free energy (kcal mol^{-1}) predictions by MM-PB(GB)SA for deprotonated 4-hydroxyl-coumarins

ID	R_1	$\Delta G_{(PB)\text{-}subt}$	$\Delta G_{(GB)\text{-}subt}$	TSTOT	$\Delta G_{(PB)\text{-}total}$	$\Delta G_{(GB)\text{-}total}$	$\log(IC_{50})$
ID49	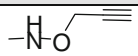	−43.96	−53.62	−24.35	−19.61	−29.27	−1.13
ID48	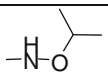	−43.59	−54.61	−25.79	−17.80	−28.82	−0.62
ID46	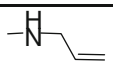	−42.51	−48.94	−25.16	−17.35	−23.78	0.10
ID47		−40.55	−48.66	−26.55	−14.00	−22.11	1.28

clorobiocin compounds (ID50 and ID44 respectively) since their pKa values were close to the physiological pH 7.4 (see Fig. 4). The rest of the compounds in the novobiocin analogues subset were considered neutral.

In most of the crystal structures available in the PDB, the flexible loop 2 has not been resolved due to disorder of the region. So far we can mention three structures, the pdb entry KIJ [20] (novobiocin ligand in *T. thermophilus* 2.30 Å), 3G7E [33] (pyrazolthiazole based ligand in *E. coli* 2.20 Å) and the very recently published structure 4DUH [34] (4,5′-bithiazole based ligand in *E. coli* 1.5 Å) whose loop 2 coordinates have been completely or partially given. In these structures some interactions have been described that contribute to the stabilization of loop 2. In the 1KIJ structure, the novobiocin interacts with residues Lys102, Phe103, Lys109 and Val117 (equivalent to Lys103, Phe104, Lys110 and Val118 in *E. coli* numbering), in 3G7E, residues Gly102, Phe104, Asp105 and Asp106 are involved in hydrophobic interactions with the pyrazolthiazole inhibitor while in 4DUH, a salt bridge formed by Lys103, Asp49 and Glu50, as well as a hydrogen bond between the amine nitrogen of the inhibitor and a carbonyl group of Gly101 are found.

Likewise, the complexes involving deprotonated 4-hydroxy-coumarins based compounds like novobiocin derivatives (ID45 to ID49) and pyrazolopyrimidine analogous (ID12 to ID20), were stable along the MD simulations. In both cases loop 2 was stabilized by interaction of the deprotonated hydroxyl either with Lys103 side chain or with Phe104 side chain (CB) in the case of novobiocin derivatives and pyrazolopyrimidines respectively (Fig. S8 in

Table 7 The influence of the different protonation states on the MD simulation and the calculation of relative binding free energy by MM-PB(GB)SA methods for 4-hydroxyl-coumarins, 4-methylamine-coumarin, 4-(1-methylpiperazine)-coumarin and 4-piperazyl-coumarin

ID/(charge)	$Log(IC_{50})$	$\Delta G_{(PB)\text{-}subt}$	$\Delta G_{(GB)\text{-}subt}$	ID/(charge)	$Log(IC_{50})$	$\Delta G_{(PB)\text{-}subt}$	$\Delta G_{(GB)\text{-}subt}$
ID49/(0)	−1.13	−38.36(4.66)	−51.69(4.34)	ID44/(0)	−0.68	***−45.04(5.68)***	***−66.86(3.40)***
ID49/(−1)	−1.13	***−43.96(4.52)***	***−53.62(4.11)***	ID44/(−1)	−0.68	−43.54(5.56)	−52.94(5.45)
ID48/(0)	−0.62	−42.35(4.12)	−51.80(3.44)	ID50/(0)	−0.39	***−39.44(4.94)***	***−44.82(4.95)***
ID48/(−1)	−0.62	***−43.59(5.25)***	***−54.61(4.73)***	ID50/(−1)	−0.39	−37.34(5.01)	−41.27(6.59)
ID45/(0)	−0.48	−29.42(3.97)	−36.45(2.84)	ID36/(0)	−0.7	***−45.82(4.20)***	***−56.93(3.22)***
ID45/(−1)	−0.48	***−39.02(5.56)***	***−41.09(4.02)***	ID36/(+1)	−0.7	−39.46(4.47)	−48.16(3.70)
ID46/(0)	0.1	−38.36(4.25)	−48.77(3.15)	ID37/(0)	−0.64	***−45.20(4.64)***	***−57.93(3.60)***
ID46/(−1)	0.1	***−42.51(5.65)***	***−48.94(4.31)***	ID37/(+1)	−0.64	−43.49(4.64)	−55.84(3.45)
ID47/(0)	1.28	−35.33(4.69)	−42.24(4.32)	ID35/(0)	−0.54	***−38.96(4.31)***	***−45.20(3.12)***
ID47/(−1)	1.28	***−40.55(4.34)***	***−48.66(3.36)***	ID35/(+1)	−0.54	−34.43(4.79)	−43.14(3.64)

Supplementary material). Longer residence times of interactions exhibited at protein-ligand interfaces were typically related to stronger interaction energies that were captured by MM-PB(GB)SA calculations.

However, deprotonation had a detrimental effect in the simulations involving novobiocin (ID50) and clorobiocin (ID44) where the butenylbenzamide substituent of both ligands adopted an extended conformation being accessible by the solvent.

Similar to pyrazolopyrimidine ID8, the enthalpy was underestimated for compound ID45 by MM-PB(GB)SA method because the two water molecules at the hydrophobic pocket interface were not included in the simulation. MM-PBSA technique correctly ranked compounds ID46 to ID49 identifying the more favorable effect of alkyloxy over the alkylic substituents. The entropy calculation showed that those compounds with more rigid substituents (ID49 and ID46) displayed a lower entropy penalty (shown in Table 6).

Complexes involving protonated 4-amino coumarin analogues ID35 and ID36 resulted unstable in terms of RMSD along the MD simulation (Fig. S9 in Supplementary material). Fluctuations were observed in these ligands (coumarin substructure with animo group) and residues Arg136 and Gly77 as well as a more open conformation of loop 2 leading to the loss of interactions and thus, underestimated binding free energy values derived from MM-PB(GB)SA methods. Interestingly, GyrB-ID37 complex was stable in both protonation states of the ligand (NH_2 and NH_3^+) due to interactions between the piperazyl substituent and the Asn107 side chain stabilizing loop 2 during the simulation (Fig. S9). These data suggest that the more rigid the coumarin-substituent substructure the more stable the GyrB-ligand interface interaction during the MD simulations. The relative binding free energy for the complexation involving the compounds under analysis estimated by the MM-PB(GB)SA methods is shown in Table 7 in neutral and charged states.

Conclusions

A comprehensive study of the performance of different molecular modeling tools for the *in silico* calculation of the binding free energy ΔG related to the inhibition of the DNA GyrB24 subunit of *E. coli* inhibition by a diverse set of ligands is presented. The study shows that the Lamarckian genetic algorithm as implemented in Autodock4.2 is a useful tool that can be used to predict the possible binding mode of potential new DNA GyrB inhibitors. A valuable benefit of this algorithm is its capability to handle, with adequate accuracy, the flexibility of the Asn46 side chain whose conformation is affected upon ligand binding.

However, as in the case of many docking studies on other targets, the performance of the different assessed scoring functions aimed at the prediction of the DNA GyrB24 subunit of *E. coli* inhibition was not successful in all the subsets of congeneric compounds. The study also shows that although rescoring schemes (based on MM-PB(GB)SA) introduce improvement, these techniques are of limited value when used in virtual screening. These energy calculations are very dependent on the stability of the structure along the MD simulations, which is also reliant on the stabilizing effects of the ligand on residue Arg136 and at least a few anchoring points in the flexible loop 2. In this sense we found that rigid ligand substituents close to loop 2 can have a more favorable effect on the stabilization of loop 2 which can be taken into account when designing new GyrB inhibitors.

A limitation of the MM-PB(GB)SA method is the accuracy in ranking analogues that differ in whether they have a substituent interacting with residues Val43, Ala47, Val71 and Val167 replacing two water molecules from the cavity. The technique overestimates the enthalpy contribution of large ligand substituents in this pocket compared to the energy obtained in the presence of the two water molecules.

However, the normal mode method is able to capture the entropic cost of either keeping the two water molecules in the protein-ligand interface or displacing the water molecules by flexible substituents interacting in the deep pocket. These results suggest that when designing GyrB inhibitors, the addition of planar and rigid substituents that interact with the hydrophobic pocket can have an entropic favorable contribution to the complex formation and hence to the GyrB inhibitory activity.

In general we can conclude that despite the limitations, the technique is useful to get insight into DNA GyrB ATPase inhibition that can be used to support the further rational design of inhibitors.

Acknowledgments We are very grateful to the Flemish Interuniversity Council (Belgium) for financial support to the project "Strengthening postgraduate education and research in Pharmaceutical Sciences". We would also like to thank to Prof. Wigley for the contribution to this work with the x-ray structure of the protein liganded to the GR122222X inhibitor and Prof. Dr. Dirk Kostrewa for providing the crystallographic structure of the protein bound to compounds ID5 and ID8.

References

1. Monaghan RL, Barrett JF (2006) Antibacterial drug discovery–then, now and the genomics future. Biochem Pharmacol 71(7):901–909
2. Payne DJ, Gwynn MN, Holmes DJ, Pompliano DL (2007) Drugs for bad bugs: confronting the challenges of antibacterial discovery. Nat Rev Drug Discov 6(1):29–40. doi:10.1038/nrd2201
3. The antibacterial lead discovery challenge. Nat Rev Drug Discov 9(10):751–752. doi:10.1038/nrd3289

4. Maxwell A (1997) DNA gyrase as a drug target. Trends Microbiol 5(3):102–109. doi:10.1016/S0966-842X(96)10085-8
5. Cotten M, Bresnahan D, Thompson S, Sealy L, Chalkley R (1986) Novobiocin precipitates histones at concentrations normally used to inhibit eukaryotic type II topoisomerase. Nucleic Acids Res 14(9):3671–3686
6. Sherer BA, Hull K, Green O, Basarab G, Hauck S, Hill P, Loch JT, 3rd, Mullen G, Bist S, Bryant J, Boriack-Sjodin A, Read J, DeGrace N, Uria-Nickelsen M, Illingworth RN, Eakin AE Pyrrolamide DNA gyrase inhibitors: optimization of antibacterial activity and efficacy. Bioorg Med Chem Lett 21 (24):7416–7420. doi:10.1016/j.bmcl.2011.10.010
7. Eakin AE, Green O, Hales N, Walkup GK, Bist S, Singh A, Mullen G, Bryant J, Embrey K, Gao N, Breeze A, Timms D, Andrews B, Uria-Nickelsen M, Demeritt J, Loch JT, 3rd, Hull K, Blodgett A, Illingworth RN, Prince B, Boriack-Sjodin PA, Hauck S, Macpherson LJ, Ni H, Sherer B Pyrrolamide DNA gyrase inhibitors: Fragment-based nuclear magnetic resonance screening to identify antibacterial agents. Antimicrob Agents Chemother 56 (3):1240–1246. doi:10.1128/AAC.05485-11
8. Schechner M, Sirockin F, Stote RH, Dejaegere AP (2004) Functionality maps of the ATP binding site of DNA gyrase B: generation of a consensus model of ligand binding. J Med Chem 47(18):4373–4390. doi:10.1021/jm0311184
9. Yu H, Rick SW (2009) Free energies and entropies of water molecules at the inhibitor-protein interface of DNA gyrase. J Am Chem Soc 131:6608–6613
10. Brvar M, Perdih A, Oblak M, Masic LP, Solmajer T. In silico discovery of 2-amino-4-(2,4-dihydroxyphenyl)thiazoles as novel inhibitors of DNA gyrase B. Bioorg Med Chem Lett 20 (3):958–962. doi:10.1016/j.bmcl.2009.12.060
11. Boehm HJ, Boehringer M, Bur D, Gmuender H, Huber W, Klaus W, Kostrewa D, Kuehne H, Luebbers T, Meunier-Keller N, Mueller F (2000) Novel inhibitors of DNA gyrase: 3D structure based biased needle screening, hit validation by biophysical methods, and 3D guided optimization. A promising alternative to random screening. J Med Chem 43(14):2664–2674
12. Lubbers T, Angehrn P, Gmunder H, Herzig S, Kulhanek J (2000) Design, synthesis, and structure-activity relationship studies of ATP analogues as DNA gyrase inhibitors. Bioorg Med Chem Lett 10(8):821–826
13. Goetschi E, Angehrn P, Gmuender H, Hebeisen P, Link H, Masciadri R, Nielsen J (1993) Cyclothialidine and its congeners: a new class of DNA gyrase inhibitors. Pharmacol Ther 60(2):367–380
14. Angehrn P, Buchmann S, Funk C, Goetschi E, Gmuender H, Hebeisen P, Kostrewa D, Link H, Luebbers T, Masciadri R, Nielsen J, Reindl P, Ricklin F, Schmitt-Hoffmann A, Theil FP (2004) New antibacterial agents derived from the DNA gyrase inhibitor cyclothialidine. J Med Chem 47(6):1487–1513. doi:10.1021/jm0310232
15. Laurin P, Ferroud D, Schio L, Klich M, Dupuis-Hamelin C, Mauvais P, Lassaigne P, Bonnefoy A, Musicki B (1999) Structure-activity relationship in two series of aminoalkyl substituted coumarin inhibitors of gyrase B. Bioorg Med Chem Lett 9(19):2875–2880
16. Ferroud D, Collard J, Klich M, Dupuis-Hamelin C, Mauvais P, Lassaigne P, Bonnefoy A, Musicki B (1999) Synthesis and biological evaluation of coumarincarboxylic acids as inhibitors of gyrase B. L-rhamnose as an effective substitute for L-noviose. Bioorg Med Chem Lett 9(19):2881–2886
17. Periers AM, Laurin P, Ferroud D, Haesslein JL, Klich M, Dupuis-Hamelin C, Mauvais P, Lassaigne P, Bonnefoy A, Musicki B (2000) Coumarin inhibitors of gyrase B with N-propargyloxycarbamate as an effective pyrrole bioisostere. Bioorg Med Chem Lett 10(2):161–165
18. Schio L, Chatreaux F, Loyau V, Murer M, Ferreira A, Mauvais P, Bonnefoy A, Klich M (2001) Fine tuning of physico-chemical parameters to optimise a new series of novobiocin analogues. Bioorg Med Chem Lett 11(11):1461–1464
19. Holdgate GA, Tunnicliffe A, Ward WH, Weston SA, Rosenbrock G, Barth PT, Taylor IW, Pauptit RA, Timms D (1997) The entropic penalty of ordered water accounts for weaker binding of the antibiotic novobiocin to a resistant mutant of DNA gyrase: a thermodynamic and crystallographic study. Biochemistry 36(32):9663–9673. doi:10.1021/bi970294+
20. Lamour V, Hoermann L, Jeltsch JM, Oudet P, Moras D (An open conformation of the Thermus thermophilus gyrase B ATP-binding domain) An open conformation of the thermus thermophilus gyrase B ATP-binding domain. J Biol Chem 277(21):18947–18953. doi:10.1074/jbc.M111740200
21. Lafitte D, Lamour V, Tsvetkov PO, Makarov AA, Klich M, Deprez P, Moras D, Briand C, Gilli R (2002) DNA gyrase interaction with coumarin-based inhibitors: the role of the hydroxybenzoate isopentenyl moiety and the 5′-methyl group of the noviose. Biochemistry 41 (23):7217–7223
22. Lewis RJ, Singh OM, Smith CV, Skarzynski T, Maxwell A, Wonacott AJ, Wigley DB (1996) The nature of inhibition of DNA gyrase by the coumarins and the cyclothialidines revealed by X-ray crystallography. EMBO J 15(6):1412–1420
23. Condemine G, Smith CL (1990) Transcription regulates oxolinic acid-induced DNA gyrase cleavage at specific sites on the E. coli chromosome. Nucleic Acids Res 18(24):7389–7396
24. Bostrom J, Greenwood JR, Gottfries J (2003) Assessing the performance of OMEGA with respect to retrieving bioactive conformations. J Mol Graph Model 21(5):449–462
25. Halgren TA (1999) MMFF VI. MMFF94s Option for energy minimization studies. J Comput Chem 20(7):720–729
26. MarvinSketch (2011). 5.4.1.1 edn. Copyright 1998–2011 Chemaxon Ltd.,
27. Oblak M, Kotnik M, Solmajer T (2007) Discovery and development of ATPase inhibitors of DNA gyrase as antibacterial agents. Curr Med Chem 14(19):2033–2047
28. Brino L, Urzhumtsev A, Mousli M, Bronner C, Mitschler A, Oudet P, Moras D (2000) Dimerization of Escherichia coli DNA-gyrase B provides a structural mechanism for activating the ATPase catalytic center. J Biol Chem 275(13):9468–9475
29. Saiz-Urra L, Cabrera MA, Froeyen M (2011) Exploring the conformational changes of the ATP binding site of gyrase B from Escherichia coli complexed with different established inhibitors by using molecular dynamics simulation protein-ligand interactions in the light of the alanine scanning and free energy decomposition methods. J Mol Graph Model 29(5):726–739. doi:10.1016/j.jmgm.2010.12.005
30. Saiz-Urra L, Cabrera Perez MA, Helguera AM, Froeyen M (2011) Combining molecular docking and QSAR studies for modelling the antigyrase activity of cyclothialidine derivatives. Eur J Med Chem 46(7):2736–2747. doi:10.1016/j.ejmech.2011.03.061
31. Tsai FT, Singh OM, Skarzynski T, Wonacott AJ, Weston S, Tucker A, Pauptit RA, Breeze AL, Poyser JP, O'Brien R, Ladbury JE, Wigley DB (1997) The high-resolution crystal structure of a 24-kDa gyrase B fragment from E. Coli complexed with one of the most potent coumarin inhibitors, clorobiocin. Proteins 28(1):41–52. doi:10.1002/(SICI)1097-0134(199705)28:1<41::AID-PROT4>3.0.CO;2-M
32. Ward WH, Holdgate GA (2001) Isothermal titration calorimetry in drug discovery. Prog Med Chem 38:309–376
33. Ronkin SM, Badia M, Bellon S, Grillot AL, Gross CH, Grossman TH, Mani N, Parsons JD, Stamos D, Trudeau M, Wei Y, Charifson PS (2010) Discovery of pyrazolthiazoles as novel and potent inhibitors of bacterial gyrase. Bioorg Med Chem Lett 20(9):2828–2831. doi:10.1016/j.bmcl.2010.03.052
34. Brvar M, Perdih A, Renko M, Anderluh G, Turk D, Solmajer T (2012) Structure-based discovery of substituted 4,5′-bithiazoles as

novel DNA gyrase inhibitors. J Med Chem 55(14):6413–6426. doi:10.1021/jm300395d
35. Morris GM, Huey R, Lindstrom W, Sanner MF, Belew RK, Goodsell DS, Olson AJ (2009) AutoDock4 And AutoDockTools4: Automated docking with selective receptor flexibility. J Comput Chem. doi:10.1002/jcc.21256
36. Sanner MF (1999) Python: A programming language for software integration and development. J Mol Graph Model 17(1):57–61
37. Kroemer RT, Vulpetti A, McDonald JJ, Rohrer DC, Trosset JY, Giordanetto F, Cotesta S, McMartin C, Kihlen M, Stouten PF (2004) Assessment of docking poses: Interactions-based accuracy classification (IBAC) versus crystal structure deviations. J Chem Inf Comput Sci 44(3):871–881. doi:10.1021/ci049970m
38. Pettersen EF, Goddard TD, Huang CC, Couch GS, Greenblatt DM, Meng EC, Ferrin TE (2004) UCSF chimera - a visualization system for exploratory research and analysis. J Comput Chem 25(13):1605–1612
39. McGann MR, Almond HR, Nicholls A, Grant JA, Brown FK (2003) Gaussian docking functions. Biopolymers 68(1):76–90. doi:10.1002/bip.10207
40. Verkhivker GM, Bouzida D, Gehlhaar DK, Rejto PA, Arthurs S, Colson AB, Freer ST, Larson V, Luty BA, Marrone T, Rose PW (2000) Deciphering common failures in molecular docking of ligand-protein complexes. J Comput Aided Mol Des 14(8):731–751
41. Eldridge MD, Murray CW, Auton TR, Paolini GV, Mee RP (1997) Empirical scoring functions: I. The development of a fast empirical scoring function to estimate the binding affinity of ligands in receptor complexes. J Comput Aided Mol Des 11(5):425–445
42. Stahl M, Rarey M (2001) Detailed analysis of scoring functions for virtual screening. J Med Chem 44(7):1035–1042
43. Grant JA, Pickup BT, Nicholls A (2001) A smooth permittivity function for Poisson–Boltzmann solvation methods. J Comput Chem 22(6):608–640
44. McGaughey GB, Sheridan RP, Bayly CI, Culberson JC, Kreatsoulas C, Lindsley S, Maiorov V, Truchon JF, Cornell WD (2007) Comparison of topological, shape, and docking methods in virtual screening. J Chem Inf Model 47(4):1504–1519. doi:10.1021/ci700052x
45. Vigers GP, Rizzi JP (2004) Multiple active site corrections for docking and virtual screening. J Med Chem 47(1):80–89. doi:10.1021/jm030161o
46. McGann M (2011) FRED pose prediction and virtual screening accuracy. J Chem Inf Model. doi:10.1021/ci100436p
47. Hallgren T (1996) Merck molecular force field. I. Basis, form, scope, parameterization, and performance of MMFF94. J Comp Chem 17:490–519
48. Cole JC, Murray CW, Nissink JW, Taylor RD, Taylor R (2005) Comparing protein-ligand docking programs is difficult. Proteins 60(3):325–332. doi:10.1002/prot.20497
49. Luo R, David L, Gilson MK (2002) Accelerated Poisson-Boltzmann calculations for static and dynamic systems. J Comput Chem 23(13):1244–1253. doi:10.1002/jcc.10120
50. Kollman PA, Massova I, Reyes C, Kuhn B, Huo SH, Chong L, Lee M, Lee T, Duan Y, Wang W, Donini O, Cieplak P, Srinivasan J, Case DA, Cheatham TE III (2000) Calculating structures and free energies of complex molecules: combining molecular mechanics and continuum models. Acc Chem Res 33:889–897
51. Bashford D, Case DA (2000) Generalized born models of macromolecular solvation effects. Annu Rev Phys Chem 51:129–152. doi:10.1146/annurev.physchem.51.1.129
52. Hou T, Wang J, Li Y, Wang W (2011) Assessing the performance of the MM/PBSA and MM/GBSA methods. 1. The accuracy of binding free energy calculations based on molecular dynamics simulations. J Chem Inf Model 51(1):69–82. doi:10.1021/ci100275a
53. Connolly ML (1983) Analytical molecular surface calculation. J Appl Cryst 16:548–558
54. Case DA, Darden TA, Cheatham TE III, Simmerling CL, Wang RED J, Luo R, Crowley M, Walker RC, Zhang W, Merz KM, Wang B, Hayik S, Roitberg A, Seabra G, Kolossváry I, Wong KF, Paesani F, Vanicek J, Wu X, Brozell SR, Steinbrecher T, Gohlke H, Yang L, Tan C, Mongan J, Hornak V, Cui G, Mathews DH, Seetin MG, Sagui C, Babin V, Kollman PA (2008) AMBER 10 edn. University of California, San Francisco
55. Wang J, Wang W, Kollman PA, Case DA (2006) Automatic atom type and bond type perception in molecular mechanical calculations. J Mol Graph Model 25(2):247–260. doi:10.1016/j.jmgm.2005.12.005
56. Wang J, Wolf RM, Caldwell JW, Kollman PA, Case DA (2004) Development and testing of a general amber force field. J Comput Chem 25(9):1157–1174. doi:10.1002/jcc.20035
57. Duan Y, Wu C, Chowdhury S, Lee MC, Xiong G, Zhang W, Yang R, Cieplak P, Luo R, Lee T, Caldwell J, Wang J, Kollman P (2003) A point-charge force field for molecular mechanics simulations of proteins based on condensed-phase quantum mechanical calculations. J Comput Chem 24(16):1999–2012. doi:10.1002/jcc.10349
58. Lee MC, Duan Y (2004) Distinguish protein decoys by using a scoring function based on a new AMBER force field, short molecular dynamics simulations, and the generalized born solvent model. Proteins 55(3):620–634. doi:10.1002/prot.10470
59. Jorgensen WL, Chandrasekhar J, Madura J, Klein ML (1983) Comparison of simple potential functions for simulating liquid water. J Chem Phys 79:926–935
60. Darden T, York D, Pedersen L (1993) Particle mesh Ewald-an Nlog(N) method for Ewald sums in large systems. J Chem Phys
61. Ryckaert JP, Ciccotti G, Berendsen HJC (1977) Numerical integration of the Cartesian equations of motion of a system with constraints: molecular dynamics of n-alkanes. J Comput Phys 23:327–341
62. Wang X, Sarycheva OV, Koivisto BD, McKie AH, Hof F (2008) A terphenyl scaffold for pi-stacked guanidinium recognition elements. Org Lett 10(2):297–300. doi:10.1021/ol7027042
63. Warren GL, Andrews CW, Capelli AM, Clarke B, LaLonde J, Lambert MH, Lindvall M, Nevins N, Semus SF, Senger S, Tedesco G, Wall ID, Woolven JM, Peishoff CE, Head MS (2006) A critical assessment of docking programs and scoring functions. J Med Chem 49(20):5912–5931. doi:10.1021/jm050362n
64. Brvar M, Perdih A, Oblak M, Masic LP, Solmajer T (2010) In silico discovery of 2-amino-4-(2,4-dihydroxyphenyl)thiazoles as novel inhibitors of DNA gyrase B. Bioorg Med Chem Lett 20(3):958–962. doi:10.1016/j.bmcl.2009.12.060
65. Maxwell A, Lawson DM (2003) The ATP-binding site of type II topoisomerases as a target for antibacterial drugs. Curr Top Med Chem 3(3):283–303
66. Gormley NA, Orphanides G, Meyer A, Cullis PM, Maxwell A (1996) The interaction of coumarin antibiotics with fragments of DNA gyrase B protein. Biochemistry 35(15):5083–5092. doi:10.1021/bi952888n
67. Watanabe J, Nakada N, Sawairi S, Shimada H, Ohshima S, Kamiyama T, Arisawa M (1994) Cyclothialidine, a novel DNA gyrase inhibitor. I. Screening, taxonomy, fermentation and biological activity. J Antibiot (Tokyo) 47(1):32–36
68. Chen VB, Arendall WB 3rd, Headd JJ, Keedy DA, Immormino RM, Kapral GJ, Murray LW, Richardson JS, Richardson DC (2010) MolProbity: All-atom structure validation for macromolecular crystallography. Acta Crystallogr D: Biol Crystallogr 66(1):12–21. doi:10.1107/S0907444909042073